

~~CONFIDENTIAL~~

Copy 94  
RM E50D28

NACA RM E50D28

E 50 D 28

~~53-29-52~~

~~NACA~~

TECH LIBRARY KAFB, NM  
0143617

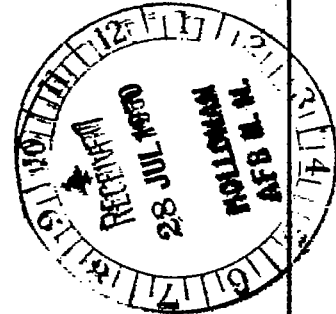
# RESEARCH MEMORANDUM

AERODYNAMIC CHARACTERISTICS OF NACA RM-10 MISSILE IN  
8- BY 6-FOOT SUPERSONIC WIND TUNNEL AT MACH  
NUMBERS FROM 1.49 TO 1.98

II - PRESENTATION AND ANALYSIS OF FORCE MEASUREMENTS

By Fred T. Esenwein, Leonard J. Obery  
and Carl F. Schueller

Lewis Flight Propulsion Laboratory  
Cleveland, Ohio



*[Handwritten signature]*

This document contains classified information affecting the National Defense of the United States within the meaning of the Espionage Act, USC 50:31 and 32. Its transmission or the revelation of its contents in any manner to an unauthorized person is prohibited by law. Information so classified may be imparted only to persons in the military and naval services of the United States, appropriate civilian officials and employees of the Federal Government who have a legitimate interest therein and to United States citizens of known loyalty and discretion who of necessity must be informed thereof.

## NATIONAL ADVISORY COMMITTEE FOR AERONAUTICS

WASHINGTON  
July 21, 1950

~~CONFIDENTIAL~~

319.98/13

~~57-297~~

0099



NACA RM E50D28

~~CONFIDENTIAL~~

## NATIONAL ADVISORY COMMITTEE FOR AERONAUTICS

RESEARCH MEMORANDUM

## AERODYNAMIC CHARACTERISTICS OF NACA RM-10 MISSILE IN

8- BY 6-FOOT SUPERSONIC WIND TUNNEL AT MACH

NUMBERS FROM 1.49 TO 1.98

## II - PRESENTATION AND ANALYSIS OF FORCE MEASUREMENTS

By Fred T. Esenwein, Leonard J. Obery  
and Carl F. Schueller

## SUMMARY

An experimental investigation to determine the aerodynamic forces acting on a slender body of revolution was conducted in the Lewis 8- by 6-foot supersonic wind tunnel. The model used was a pointed-nose rocket research missile designated by the NACA as the half-scale RM-10. Lift, drag, and pitching moment were measured for three configurations: body alone, body with two fins, and body with four fins, at free-stream Mach numbers of 1.49, 1.59, 1.78, and 1.98 for a range of angles of attack from  $0^\circ$  to  $9^\circ$ . The investigation was conducted at a Reynolds number of approximately 30,000,000 based on the body length.

The experimental results of the investigation showed that the drag coefficient increased with angle of attack but remained essentially independent of Mach number for all configurations. The lift coefficient increased with Mach number for the body alone but decreased for the body with fins. The resulting pitching-moment coefficient increased almost linearly with angle of attack for the body alone and was independent of Mach number. For the body with fins, however, the negative pitching-moment coefficient increased with angle of attack and decreased with Mach number.

The experimental force and moment coefficients for the body alone were compared with linearized potential theory and with the semiempirical method of reference 1, which includes the effect of viscosity. The results of this comparison indicate that potential theory predicted the pressure drag at zero angle of attack; however, the lift, the center of pressure location, and the increment of drag due to angle of attack were much more accurately predicted by the method of reference 1.

~~CONFIDENTIAL~~

57-377

A breakdown of the total drag coefficient at zero angle of attack indicates that the pressure drag is approximately 30 percent, the base-pressure drag is 20 percent, and the skin-friction drag is 50 percent of the total drag for this model.

### INTRODUCTION

Various theories and semiempirical methods are available for calculating the aerodynamic characteristics of bodies of revolution at supersonic speeds. Lack of experimental data for large-scale models at high Reynolds numbers and moderate angles of attack, however, has prevented an evaluation of the limitations of these theories and methods.

The purposes of this investigation were (1) to obtain force and moment data on a specific body of revolution with and without fins and to compare the values calculated by linearized potential theory and the method of reference 1 with experimentally determined force and moment coefficients for the body alone; and (2) to contribute aerodynamic data for comparison with results being obtained from other wind-tunnel and free-flight investigations of this model at different Reynolds numbers. Lift, drag, and pitching moment were measured for various body-fin combinations for a range of free-stream Mach numbers and angles of attack. The Reynolds number based on body length was 29.1, 29.2, 29.5, and  $31.1 \times 10^6$  for Mach numbers of 1.49, 1.59, 1.78, and 1.98, respectively.

### SYMBOLS

The following symbols are used in this report:

A	axial force'
b	radius of body at any station x
$C_A$	axial force coefficient, $A/q_0S$
$C_D$	drag coefficient, $D/q_0S$
$C_{D,b}$	base-pressure drag coefficient, $\frac{(p-p_0)}{q_0} \frac{S_b}{S} \cos \alpha$
$\Delta C_D$	increment of drag coefficient due to angle of attack

$\Delta C_{D,F}$	increment of fore drag coefficient, $(\Delta C_D - \Delta C_{D,b})$
$C_F$	skin-friction coefficient, based on wetted area
$C_L$	lift coefficient, $L/q_0S$
$C_{L,\alpha}$	$dC_L/d\alpha$
$C_N$	normal force coefficient, $N/q_0S$
$C_m$	pitching-moment coefficient, $m/q_0Sl$
$C_p$	pressure coefficient, $(p-p_0)/q_0$
D	drag
d	center of pressure location ahead of center of moments
G	plan-form area
h	axial distance from nose of model to center of moments
L	lift
l	length of body
M	Mach number
m	pitching moment about station of maximum cross section
N	normal force
p	static pressure
q	dynamic pressure, $\frac{\gamma}{2} pM^2$
R	Reynolds number, $\rho Ul/\mu$
S	maximum cross-sectional area
s	cross-sectional area of body at any station x
t/c	airfoil thickness to chord ratio
$U_0$	free-stream velocity

V	volume
W	wetted area
x	distance from nose of model
x,r, $\theta$	cylindrical coordinates in terms of axes fixed to body
$x_G$	distance from nose of model to centroid of plan-form area
$\alpha$	angle of attack
$\beta$	cotangent of Mach angle, $\sqrt{M^2-1}$
$\gamma$	ratio of specific heats, 1.40
$\mu$	viscosity
$\rho$	density
$\phi$	velocity potential

## Subscripts:

b	base of model
c	cross flow
f	friction
p	pressure
s	surface of model
0	free-stream conditions
1	conditions for model at zero angle of attack
2	conditions for model at angle of attack

## APPARATUS AND PROCEDURE

A photograph of the model used in this investigation is shown in figure 1. The basic parabolic body had a maximum diameter of 6 inches and a fineness ratio of 15; however, removal of the aft

1315  
portion to provide for the rocket jet in the free-flight missile resulted in a fineness ratio of 12.2. The body was blunted slightly by removal of 1/4 inch from the nose (fig. 2), which resulted in an over-all body length of 73 inches.

Sweptback stabilizing fins of circular arc profile and thickness to chord ratio of 0.10 were attached to the model during the tests of the body with fins. The fins had a taper ratio of 1.0 and an angle of sweepback of 60°.

The model was rigidly connected to a three-component strain-gage balance located inside the body and the balance was attached to the tunnel sting-strut combination. Thus only normal and axial forces and moments on the model were recorded and no tare corrections were required.

The strain-gage balance design originated at the Ames laboratory. Static calibration indicated that interaction effects between the three components were negligible and that the accuracy of the balance was of the order of 2 percent. The effects of temperature variation were avoided by maintaining the balance at a constant temperature.

A pendulum-type angle of attitude indicator mounted in the nose of the model was used to measure the angle of attack within 0.10°.

The static pressure was measured on the base of the model at the two points indicated in figure 2.

The three model configurations investigated were: body alone, body plus four fins, and body plus two horizontal fins. Each configuration was investigated through a range of Mach numbers from 1.49 to 1.98 and at angles of attack from 0° to 9°, unless model-sting fouling occurred at a lower angle of attack.

#### METHODS OF COMPUTATION AND REDUCTION OF DATA

The theoretical lift, drag, and pitching moment of the body alone were computed by means of the linearized potential theory. Equation (7) of reference 2 expresses the theoretical pressure distributions as

$$C_p = C_{p,1} + C_{p,2}$$

where

$$C_{p,1} = -\frac{2}{U_0} \frac{\partial \phi_1}{\partial x} - \left(\frac{db}{dx}\right)^2$$

and

$$C_{p,2} = 4\alpha \cos \theta \frac{db}{dx} + \alpha^2(1-4 \sin^2 \theta)$$

(1)

$C_{p,1}$  is the pressure coefficient at zero angle of attack and  $C_{p,2}$  is the additive contribution at angle of attack. For the body discussed herein, which is defined by the equation

$$b = x \sqrt{c/2} \left(2 - x/45\right)$$

where

$$0 \leq x \leq 73.25$$

and

$$c = 2/(15)^2$$

(2)

reference 2 has shown that the perturbation velocity component on the body surface is expressed as

$$\frac{\partial \phi_1}{\partial x} = -U_0 c \left\{ \frac{3-9\left(\frac{x}{45} - 1\right)}{2} \sqrt{\left(\frac{x}{45}\right)^2 - \beta^2 \left(\frac{b}{45}\right)^2} + \left[ 3 \left(\frac{x}{45} - 1\right)^2 - 1 + \frac{3}{2} \beta^2 \left(\frac{b}{45}\right)^2 \right] \cosh^{-1} \frac{x}{b\beta} \right\}$$

(3)

Lift and drag coefficients were obtained by resolving the normal and axial force coefficients into components perpendicular and parallel to the free-stream direction. For the determination of the normal force, only the increment of pressure coefficient due to angle of attack need be considered and the normal force coefficient can be expressed as

$$C_N = \frac{2}{S} \int_0^l \int_0^\pi C_{p,2} b \cos \theta \, d\theta \, dx \quad (4)$$

In this equation the integral corresponding to the term  $\alpha^2(1-4 \sin^2 \theta)$  is zero and the resulting normal force coefficient becomes

$$C_N = \frac{2\alpha S_b}{S} \quad (5)$$

where  $\alpha$  is measured in radians.

In a similar manner, the coefficient of moment about the station of maximum cross section can be expressed as

$$C_m = \frac{2}{S l} \int_0^l \int_0^\pi C_{p,2} b(h-x) \cos \theta \, d\theta \, dx \quad (6)$$

where  $h$  is the distance from the nose of the body to the station of maximum cross section. The final equation for the moment coefficient is

$$C_m = \frac{2\alpha}{S l} \left[ l(S_m - S_b) + h S_b \right] \quad (7)$$

where  $S_m$  represents the mean cross-sectional area of the body. The center of pressure location obtained by dividing the moment by the normal force is

$$d = \frac{l}{S_b} (S_m - S_b) + h \quad (8)$$

The equation for the axial pressure force coefficient excluding the pressure force on the base can be written as

$$C_{A,p} = \frac{2}{S} \int_0^l \int_0^\pi C_{p,2} b \frac{db}{dx} \, d\theta \, dx \quad (9)$$

In this case, the integral of the term  $4\alpha \cos \theta \frac{db}{dx}$  is zero, and the remaining terms yield the equation

$$C_{A,p} = (C_{D,p})_{\alpha=0} - \frac{\alpha^2 S_b}{S} \quad (10)$$

Resolving the normal and axial force coefficients, as given by equations (5) and (10), into components perpendicular and parallel to the free-stream direction gives the final relations for the lift and drag coefficients as

$$C_L = \frac{2\alpha S_b}{S} \cos \alpha - \frac{\alpha^2 S_b}{S} \sin \alpha \approx \frac{2\alpha S_b}{S} - \frac{\alpha^3 S_b}{S} \approx \frac{2\alpha S_b}{S} \quad (11)$$

$$C_{D,p} = (C_{D,p})_{\alpha=0} - \alpha^2 \frac{S_b}{S} \cos \alpha + 2\alpha \frac{S_b}{S} \sin \alpha \approx (C_{D,p})_{\alpha=0} + \frac{\alpha^2 S_b}{S} \quad (12)$$

Equation (11) agrees with the value of the lift coefficient obtained by Tsien in reference 3. The value of  $(C_{D,p})_{\alpha=0}$  in equation (12) was determined by graphically integrating the theoretical pressure distribution over the surface of the body from  $x=0$  to  $x=l$  at zero angle of attack.

The force and moment coefficients were also computed by the method of reference 1. In this method, a viscous cross flow is added to Munk's potential solution to determine the forces acting on a body inclined to the free stream. The equations as given in reference 1 for the force and moment coefficients are

$$C_L = 2 \left( \frac{S_b}{S} \right) \alpha + \eta c_{d,c} \frac{G}{S} \alpha^2 \quad (13)$$

$$\Delta C_D = \left( \frac{S_b}{S} \right) \alpha^2 + \eta c_{d,c} \frac{G}{S} \alpha^3 \quad (14)$$

$$C_m = \frac{2}{S l} \left[ v - S_b (l-h) \right] \alpha + \frac{\eta c_{d,c}}{S l} G (h-x_G) \alpha^2 \quad (15)$$

In the preceding equations,  $\eta$  is a constant depending on the body shape and  $c_{d,c}$  is the experimentally determined section drag coefficient of a circular cylinder of radius  $b$  at the cross-flow Mach number and Reynolds number. Based on the conditions of this investigation,  $\eta$  was obtained from reference 1 as 0.71 and an average value of  $c_{d,c}$  of 1.2 was selected for the range of cross-flow Reynolds numbers.

Calculations for a theoretical skin-friction coefficient  $C_f$  at zero angle of attack were made using the relation for turbulent flow over a smooth flat plate as given by von Kármán in reference 4, where

$$C_f = 0.072 \frac{1}{R^{0.2}} \quad (16)$$

based upon the wetted area. In this equation, the free-stream Reynolds number  $R$  is evaluated with the model length as the characteristic dimension.

The calculated values of  $C_f$  were converted to a skin-friction drag coefficient based upon the maximum cross-sectional area by means of the relation

$$(C_{D,f})_{\alpha=0} = C_f \frac{W}{S} \quad (17)$$

The normal and axial forces measured by the strain-gage balance were resolved into lift and drag components by the relations

$$L = N \cos \alpha - A \sin \alpha \quad (18)$$

$$D = A \cos \alpha + N \sin \alpha \quad (19)$$

Drag increments of 0.020 at a Mach number of 1.49 and 0.006 at a Mach number of 1.59 were added to the measured drag coefficients to correct for an axial pressure gradient in the tunnel test section.

Data presented in reference 5 indicate that the sting interference effect on drag is probably negligible for the ratio of sting diameter to base diameter (0.66) of this model. The data in reference 5 also indicate that the pressures over the boattail of the body are unaffected by changes in the support configuration when the boundary layer is turbulent in the region of the base, as it was in this investigation. In view of these results, no corrections for support interference were considered necessary to the data presented herein.

The drag measured by the balance for the body alone at zero angle of attack was compared with the sum of the drag components: base-pressure, pressure, and skin-friction drags. Base-pressure drag was computed from the measured base pressures and pressure drag was determined by graphical integration of the measured pressures reported in reference 2. The effect of the tunnel pressure gradient previously mentioned was evaluated and appropriate corrections have been applied to the data. At a Mach number of 1.49, corrections of 0.006 and 0.014 were added to the measured base-pressure and pressure drag coefficients, respectively; at a Mach number of 1.59 a correction of 0.006 was added to the pressure drag coefficient. No corrections were required at the higher Mach numbers.

The skin-friction drag was determined by calculating the change in momentum of the boundary layer based on the measurements presented in reference 2. Inasmuch as the boundary-layer growth along the model was not measured, corrections for the effect of the pressure distribution could not be evaluated for these data. Calculations based on an assumed linear rate of boundary-layer growth along the model, however, indicate that the correction might increase the skin-friction drag coefficient as much as 5 percent. In the reduction of the data, the static pressure and the total temperature were assumed constant through the boundary layer and the recorded total pressures were assumed to act at the geometric center of each tube.

## RESULTS AND DISCUSSION

### Body Alone

The variation of the aerodynamic coefficients with angle of attack and Mach number are presented in figures 3 and 4, respectively. The lift curve slope increases with angle of attack and Mach number (figs. 3(a) and 4(a)) and is much greater at all Mach numbers than would be predicted by linearized potential theory. The method of reference 1 predicts the trend of the variation of lift coefficient with angle of attack but underestimates the absolute value at the higher Mach numbers. At a Mach number of 1.98 and an angle of attack of  $9^\circ$ , the lift coefficient was underestimated approximately 17 percent.

The pitching-moment coefficient varied almost linearly with angle of attack (fig. 3(b)) but was unaffected by Mach number (fig. 4(b)). Inasmuch as the previous discussion showed an increase in  $C_{L,\alpha}$  with angle of attack and Mach number, the center of pressure would be expected to move rearward as shown in figures 3(c) and 4(c). The method of reference 1 overestimates the pitching moment

more than potential theory does (fig. 3(b)). Because the lift was predicted much more accurately by the method of reference 1, however, the resulting center of pressure location is in closer agreement with the measured values (fig. 3(c)).

The data in figures 3(d) and 4(d) show that the drag coefficient increased with angle of attack but was essentially independent of Mach number. As shown subsequently, from 17 to 32 percent of the increment of drag coefficient due to angle of attack can be attributed to the change in base-pressure drag with angle of attack. Inasmuch as neither the method of reference 1 nor potential theory accounts for this variation, the increments of fore drag  $\Delta C_{D,F}$  have also been plotted in figure 3(d). Comparison of the results shows that the increment of fore drag was predicted much more accurately by the method of reference 1 than by potential theory.

A comparison of pressure drag coefficients determined by potential theory and computed from the measured pressures at zero angle of attack is shown in figure 5(a). Very close agreement was obtained at all Mach numbers. A comparison of measured and calculated skin-friction drag coefficients at various Mach numbers is presented in figure 5(b). The value of skin-friction drag coefficient calculated by von Kármán's equation for turbulent flow over a smooth flat plate overestimates the experimentally determined values approximately 3 percent at a Mach number of 1.49 and 9 percent at a Mach number of 1.98. Inasmuch as the calculated values are based on incompressible two-dimensional flow, the agreement with the experimental results is probably incidental.

The data of reference 2 have been analyzed to determine the contribution of base-pressure, pressure, and skin-friction drags to the total drag at zero angle of attack, and to compare the sum of the calculated drags with the measured value. As shown in figure 6, the base-pressure drag coefficient is approximately 20 percent, the pressure drag coefficient is approximately 30 percent, and the skin-friction drag coefficient is approximately 50 percent of the total drag coefficient for this model. The summation of the calculated values agrees within 4 percent with the total drag coefficient measured with the strain-gage balance.

#### Body Plus Fins

The aerodynamic characteristics of the body plus four fins are shown in figures 7 and 8 as a function of angle of attack and Mach number, respectively. The lift curve slope increased with angle of

attack at all Mach numbers (fig. 7(a)). For a given angle of attack, however, the lift coefficient decreased with increasing Mach number (fig. 8(a)). Inasmuch as the body-alone lift increased with Mach number, the decrease in lift for the body with fins is believed to be due primarily to a loss of fin lift, although interference effects may also be significant.

The variations of pitching-moment coefficient and center of pressure with angle of attack and Mach number are presented in figures 7(b), 7(c), 8(b), and 8(c). The slope of the pitching-moment curve decreased with angle of attack at all Mach numbers and at a given angle of attack the static stability decreased as the Mach number increased. The increase in pitching-moment coefficient with Mach number was accompanied by a slight forward movement of the center of pressure as the Mach number increased from 1.49 to 1.98.

The drag coefficient increased rapidly with angle of attack due to the lift of the fins (fig. 7(d)) but remained essentially independent of Mach number (fig. 8(d)).

Removal of the two vertical fins had a negligible effect on the lift and pitching-moment characteristics for the range of Mach numbers and angles of attack of this investigation; however, the drag coefficient (fig. 7(d)) was decreased approximately 0.050. This decrement of drag coefficient was independent of Mach number and angle of attack.

The variation of base-pressure drag coefficient with angle of attack and Mach number is shown in figure 9 for the body alone and the body plus four fins. The base-pressure drag coefficient was essentially independent of Mach number at zero angle of attack. At angle of attack, however, the base-pressure drag coefficient decreased slightly with increasing Mach number but increased appreciably with angle of attack. As previously mentioned for the body alone, the increment of base-pressure drag coefficient at an angle of attack of  $9^\circ$  accounts for 32 and 17 percent of the total increment of drag coefficient at Mach numbers of 1.49 and 1.98, respectively.

The hysteresis effect (difference between values obtained with increasing and decreasing angles of attack) was reproducible. No adequate explanation of this phenomenon is available, but it is believed to be associated with separation of the cross flow. The hysteresis increased with Mach number for all configurations and was much greater for the body plus four fins. At a Mach number of 1.98 and an angle of attack of  $9^\circ$ , the hysteresis was approximately 15 percent for the body plus four fins.

## SUMMARY OF RESULTS

The aerodynamic characteristics of a slender pointed-nose body of revolution were investigated in the NACA Lewis 8- by 6-foot supersonic wind tunnel at a Reynolds number of approximately 30,000,000 and at Mach numbers of 1.49, 1.59, 1.78, and 1.98 through a range of angles of attack. From this investigation, the following results were obtained:

1. The body-alone investigation indicates that linearized potential theory accurately predicted the pressure drag at zero angle of attack. At angle of attack, however, potential theory overestimated the moment and underestimated the lift and the increment of drag due to angle of attack.

2. The method of reference 1 predicted the correct trend of the data but overestimated the pitching moment and underestimated the lift and the increment of drag at the higher Mach numbers. A comparison of the results indicates that the method of reference 1 predicted the variation of the lift, center of pressure location, and the increment of drag with angle of attack much more accurately than did potential theory.

3. The skin-friction drag coefficient for this model was predicted reasonably well by von Karman's equation for incompressible turbulent flow over a smooth flat plate.

4. The body lift coefficient increased, whereas the body-plus-fin lift coefficient decreased with increasing Mach number.

5. The pitching-moment coefficient for the body alone was unaffected by Mach number, whereas the pitching-moment coefficient for the body plus fins increased with increasing Mach number.

6. The drag coefficient for all the configurations remained essentially constant with Mach number. Removal of the vertical fins from the body decreased the drag coefficient approximately 0.050 at all angles of attack and Mach numbers.

7. A breakdown of the measured drag coefficient into three components for the body alone at an angle of attack of  $0^\circ$  indicates that for this body the base-pressure drag was approximately 20 percent, the pressure drag was approximately 30 percent, and the skin-friction drag was approximately 50 percent of the total measured drag.

8. For all configurations, the base-pressure drag coefficient increased with angle of attack but decreased slightly with increasing Mach number at angle of attack. The hysteresis effect and the absolute values of the base-pressure drag coefficient were greater for the body plus four fins than for the body alone.

Lewis Flight Propulsion Laboratory,  
National Advisory Committee for Aeronautics,  
Cleveland, Ohio.

#### REFERENCES

1. Allen, Julian H.: Estimation of the Forces and Moments Acting on Inclined Bodies of Revolution of High Fineness Ratio. NACA RM A9I26, 1949.
2. Luidens, Roger W., and Simon, Paul C.: Aerodynamic Characteristics of NACA RM-10 Missile in 8- by 6-Foot Supersonic Wind Tunnel at Mach Numbers from 1.49 to 1.98. I - Presentation and Analysis of Pressure Measurements (Stabilizing Fins Removed). NACA RM E50D10, 1950.
3. Tsien, Hsue-Shen: Supersonic Flow over an Inclined Body of Revolution. Jour. Aero. Sci., vol. 5, no. 12, Oct. 1938, pp. 480-483.
4. von Kármán, Th.: On Laminar and Turbulent Friction. NACA TM 1092, 1946.
5. Perkins, Edward W.: Experimental Investigation of the Effects of Support Interference on the Drag of Bodies of Revolution at a Mach Number of 1.5. NACA RM A8B05, 1948.

~~CONFIDENTIAL~~

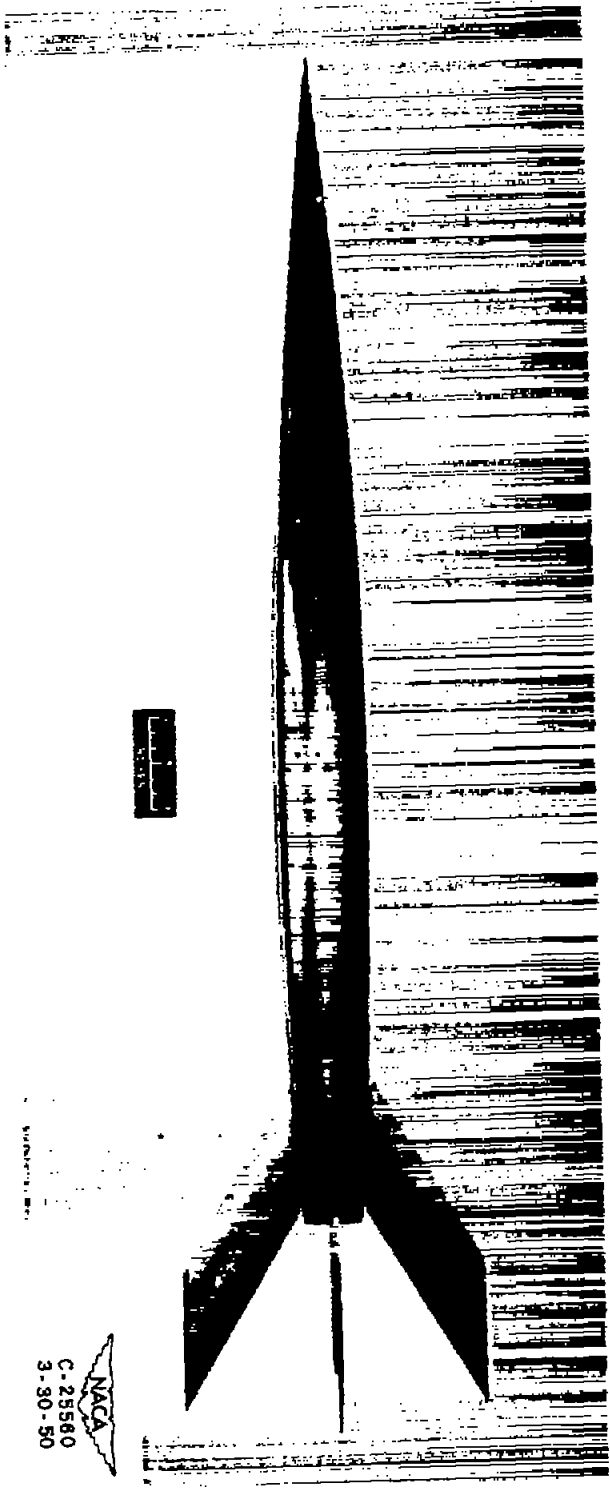


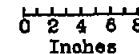
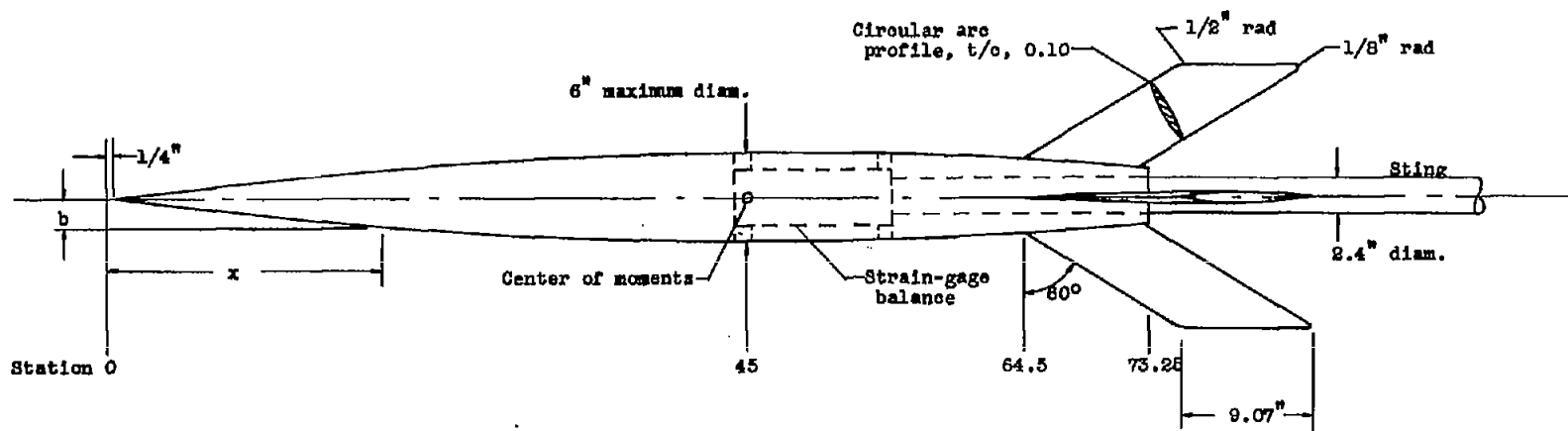
Figure 1. - NACA half-scale RM-10 missile.

NACA  
C-29580  
3-30-50

~~CONFIDENTIAL~~

NACA RM E50D28





Body profile equation:

$$b = x \sqrt{c/E} (E - x/45)$$

where

$$0 \leq x \leq 73.25$$

and

$$c = 2/(15)^2$$

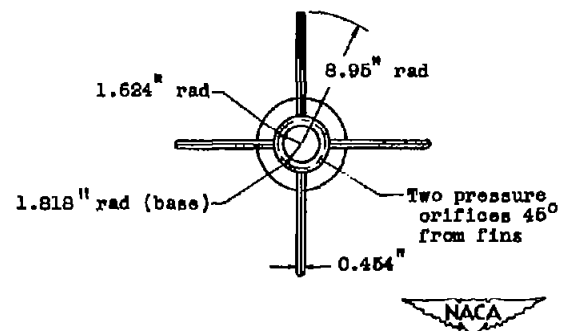
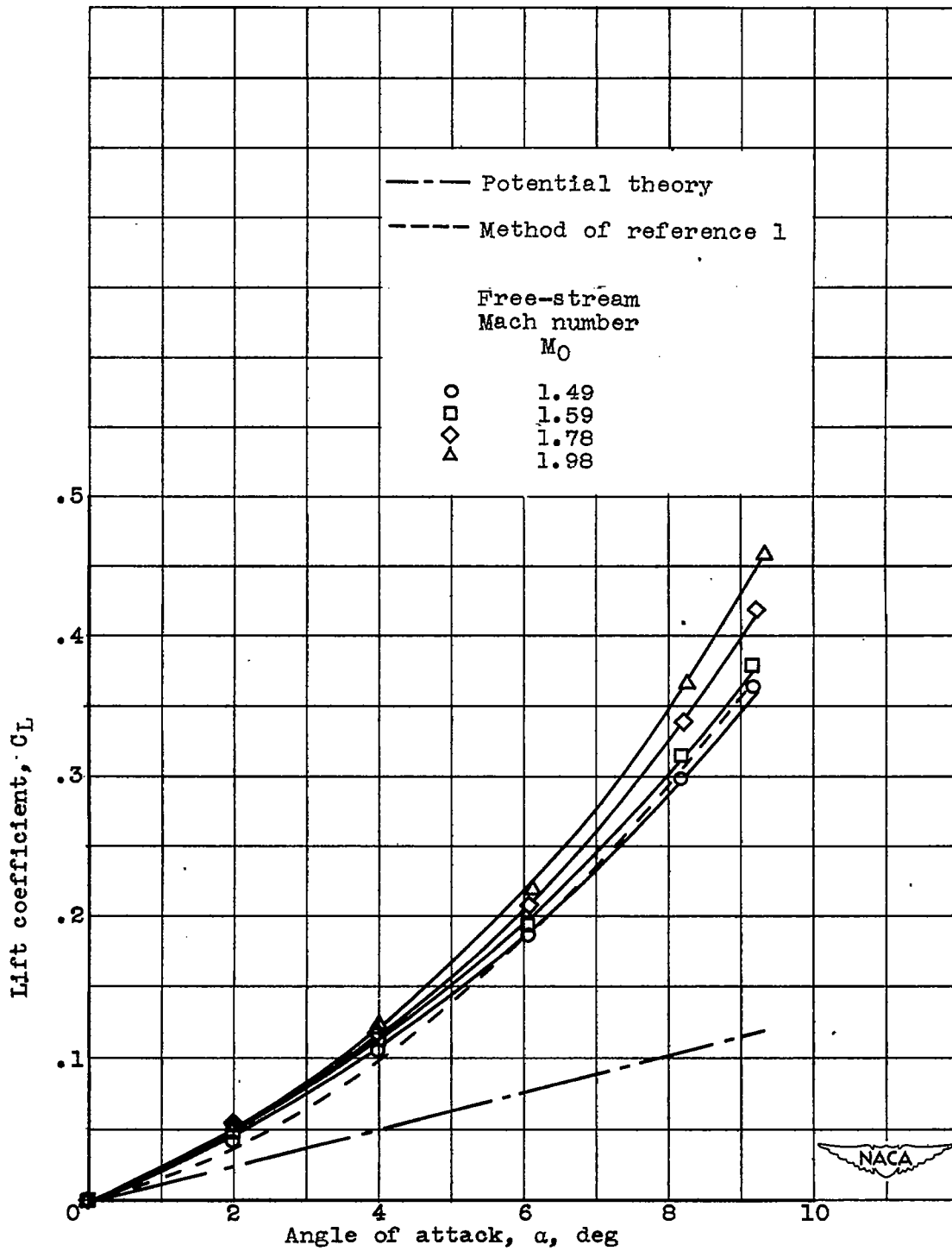
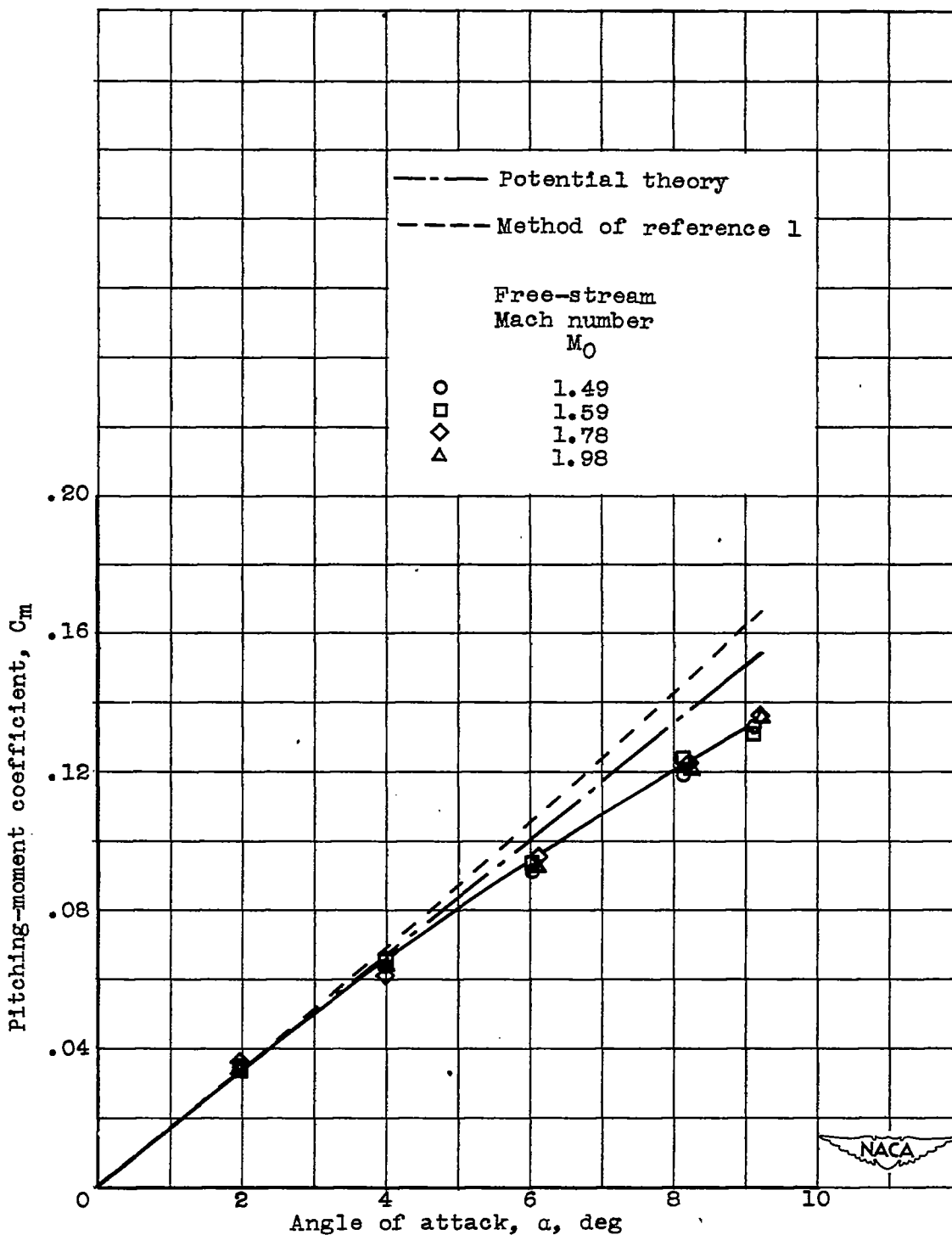


Figure 2. - Schematic diagram of half-scale model of NACA RM-10 showing principal dimensions. Wetted area (excluding base), 1033 square inches; volume, 1291 cubic inches.



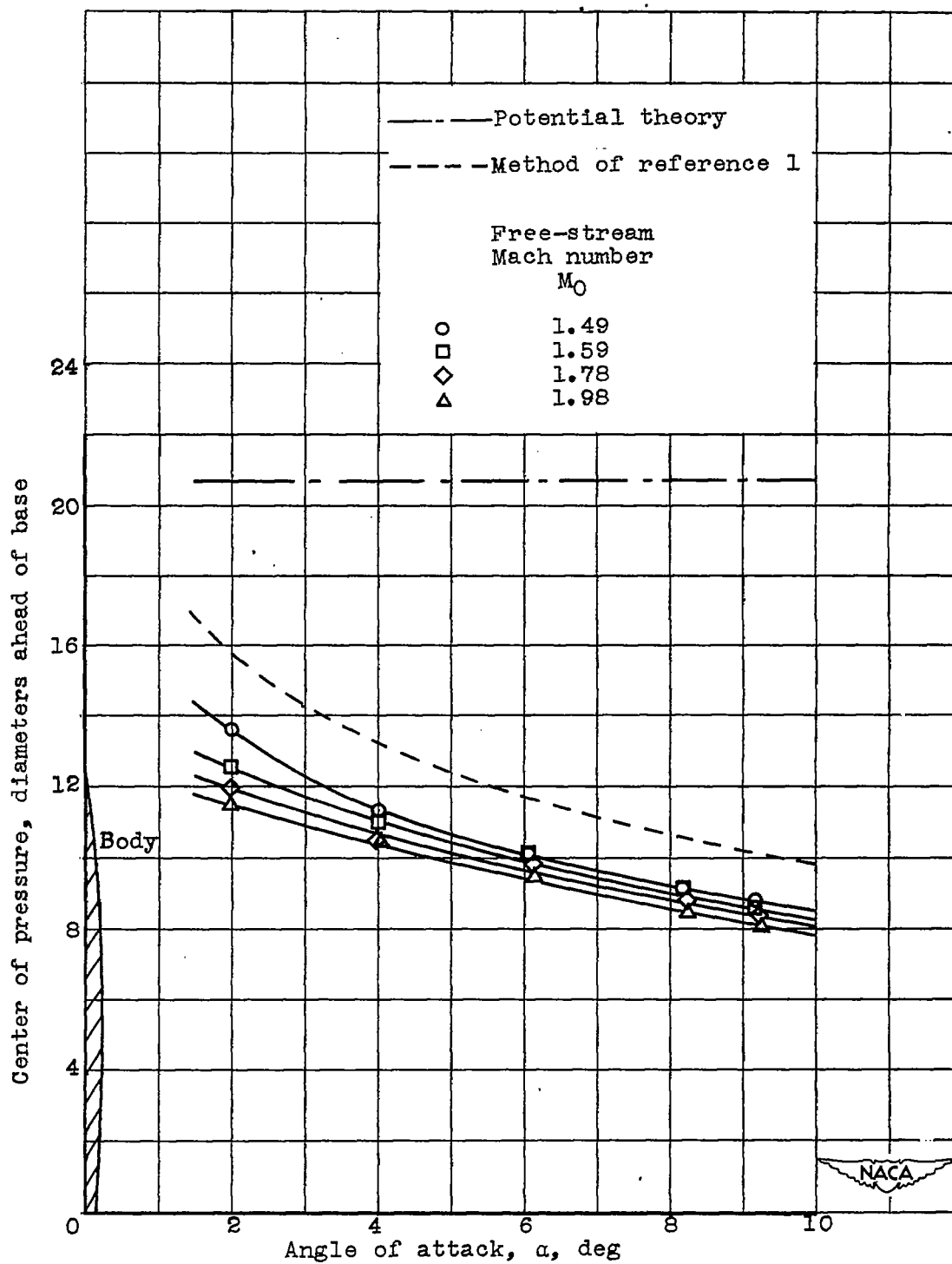
(a) Lift coefficient.

Figure 3. - Variation of aerodynamic characteristics with angle of attack at four Mach numbers for body alone.



(b) Pitching-moment coefficient.

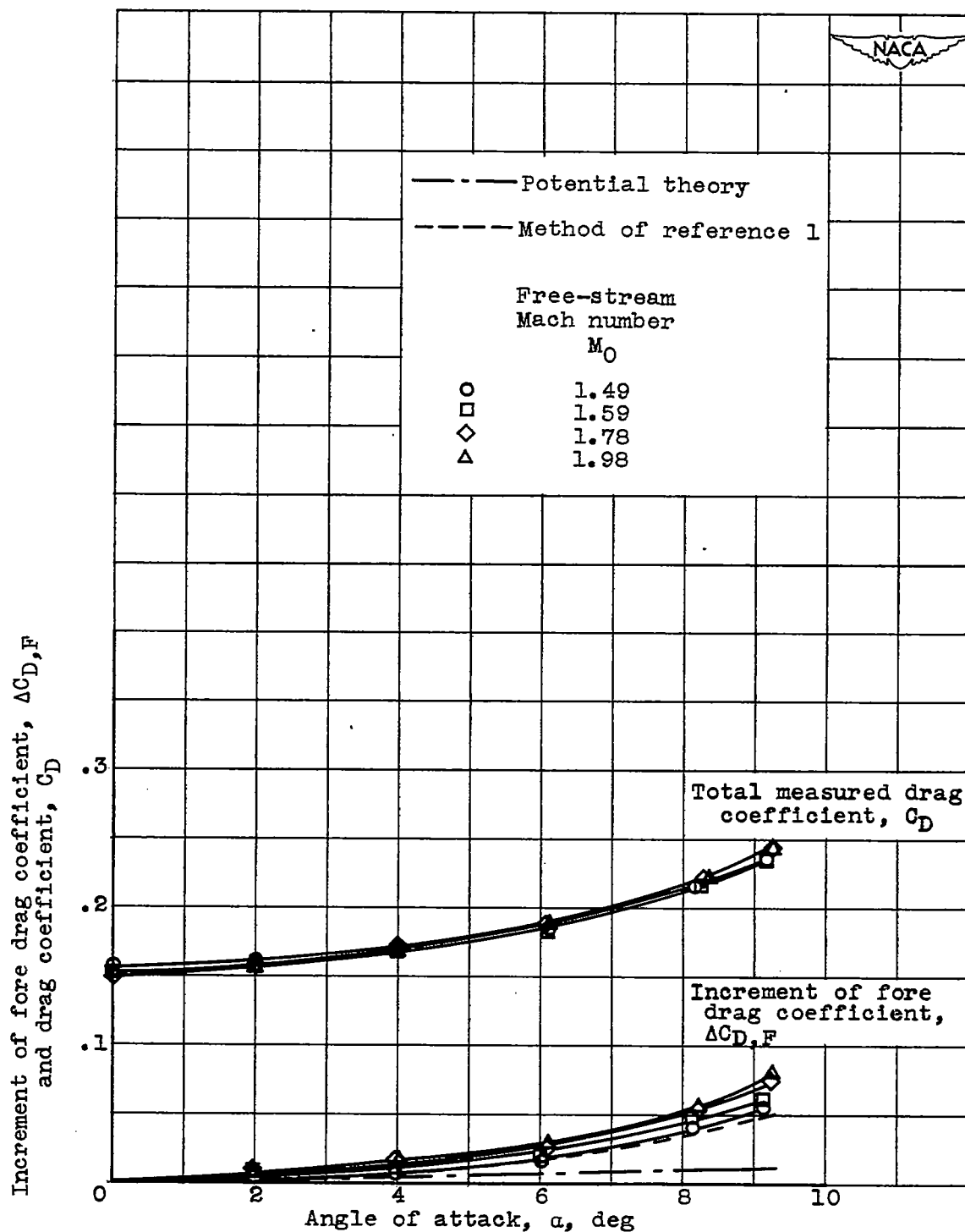
Figure 3. - Continued. Variation of aerodynamic characteristics with angle of attack at four Mach numbers for body alone.



(c) Center of pressure.

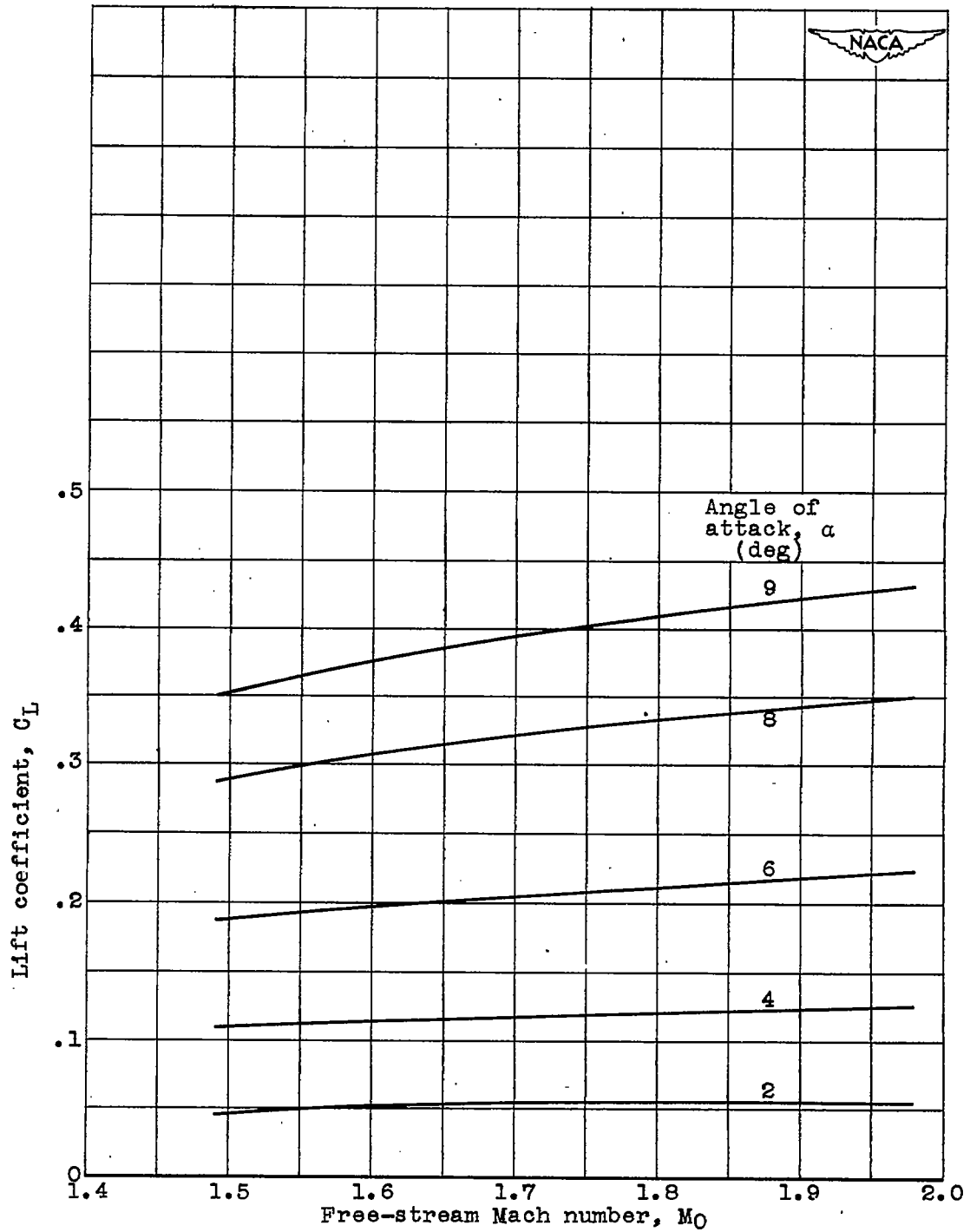
Figure 3. - Continued. Variation of aerodynamic characteristics with angle of attack at four Mach numbers for body alone.

1315



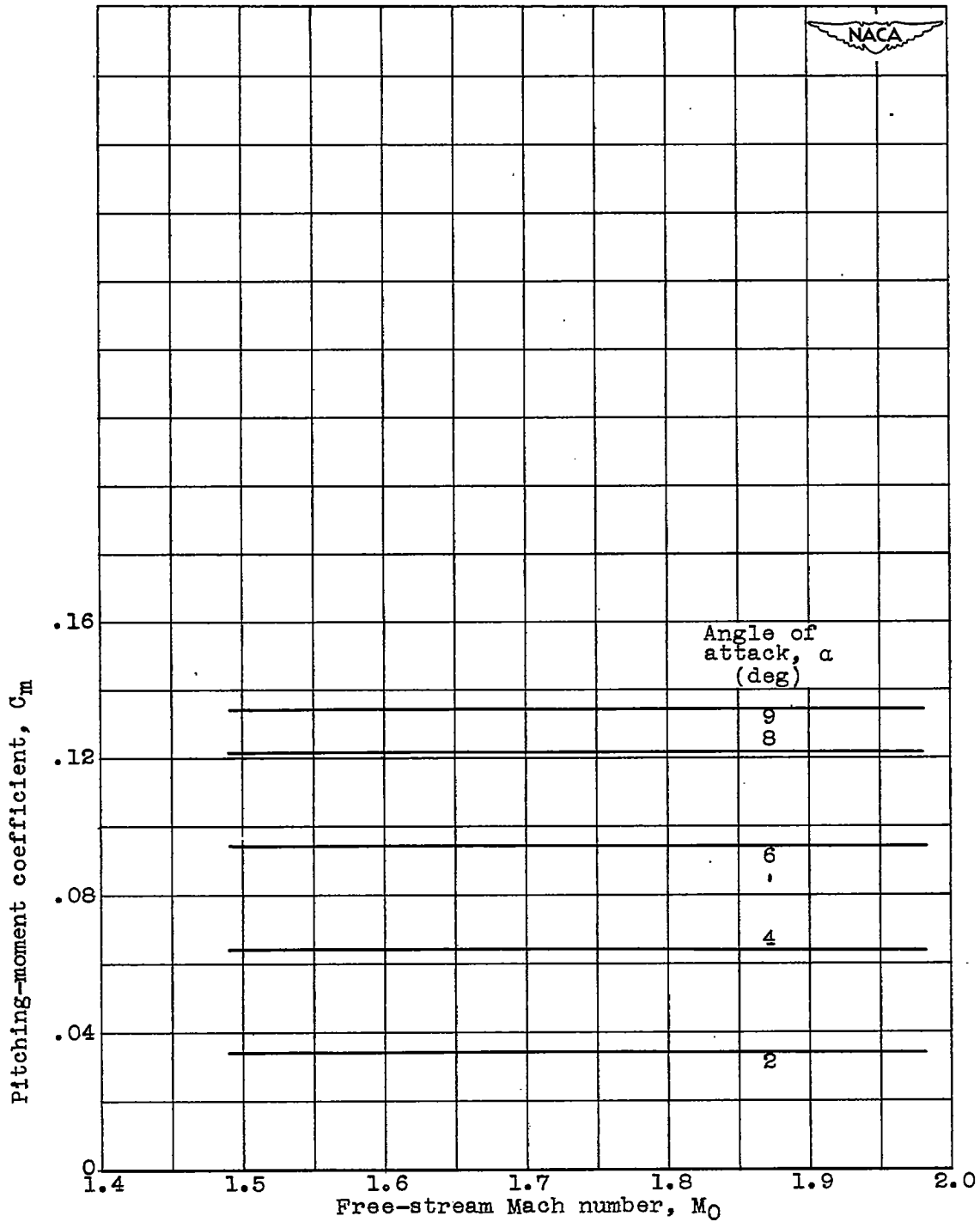
(d) Drag coefficient.

Figure 3. - Concluded. Variation of aerodynamic characteristics with angle of attack at four Mach numbers for body alone..



(a) Lift coefficient.

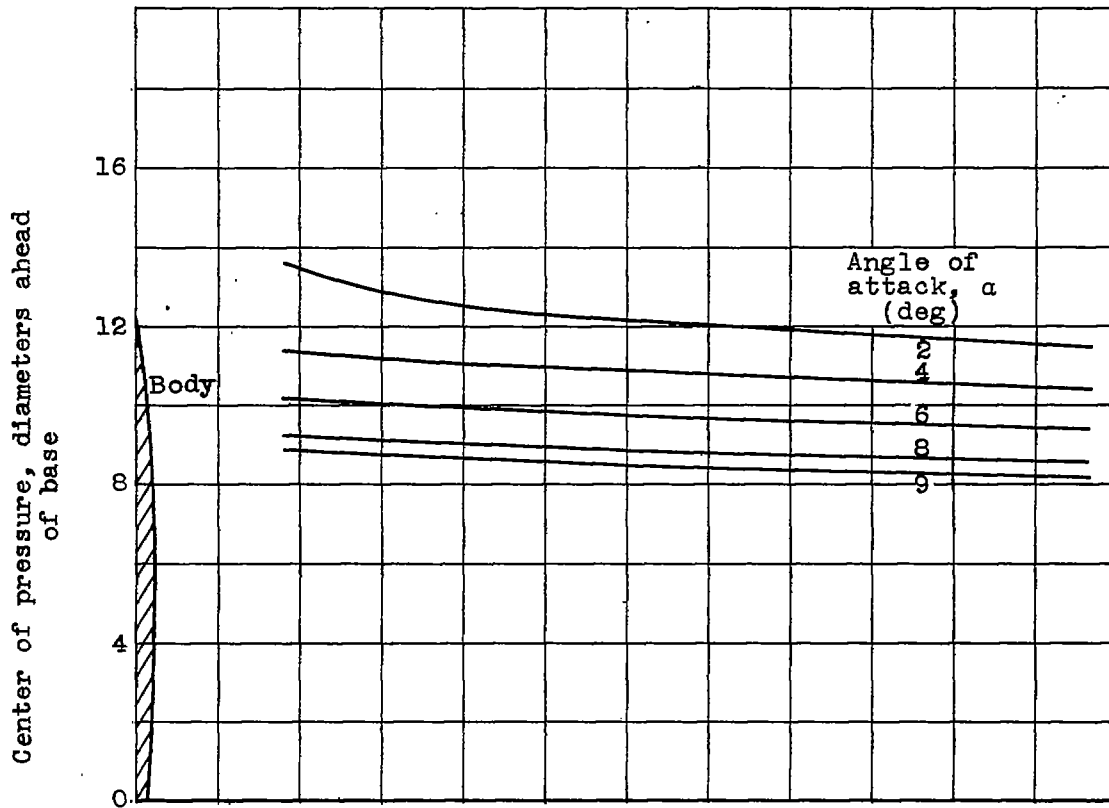
Figure 4. - Variation of aerodynamic characteristics with Mach number at various angles of attack for body alone.



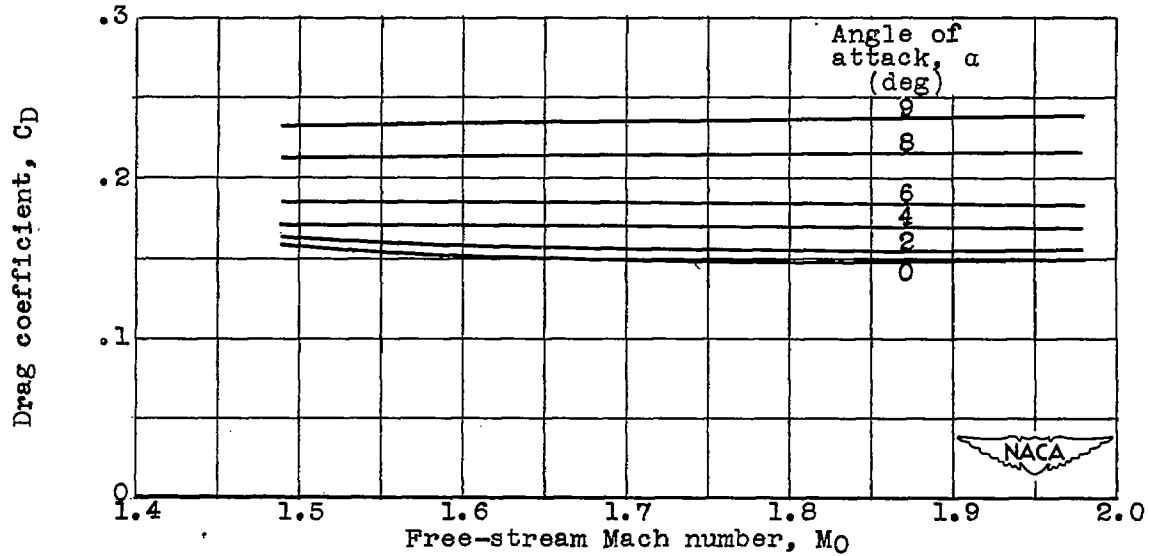
(b) Pitching-moment coefficient.

Figure 4. - Continued. Variation of aerodynamic characteristics with Mach number at various angles of attack for body alone.

1315

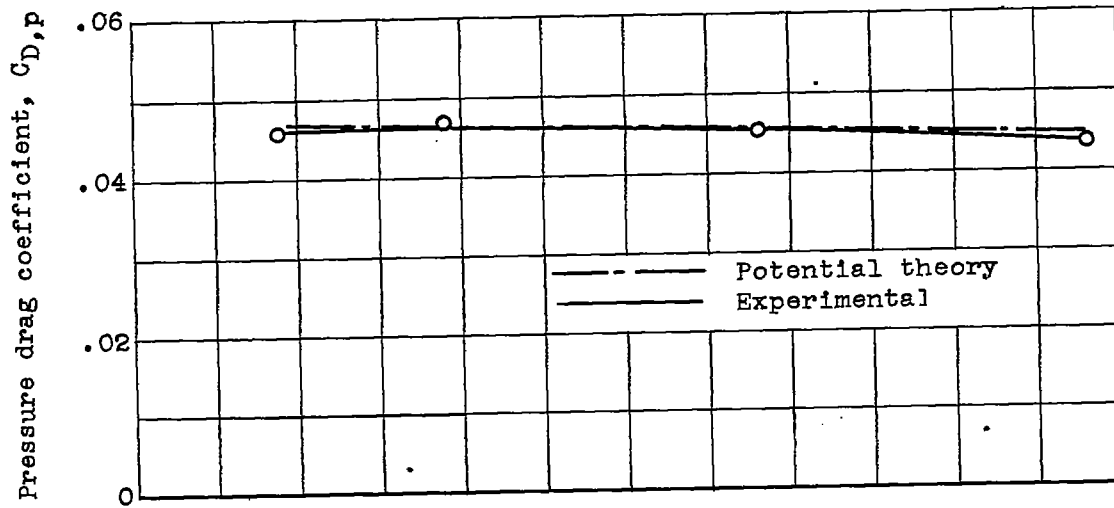


(c) Center of pressure.

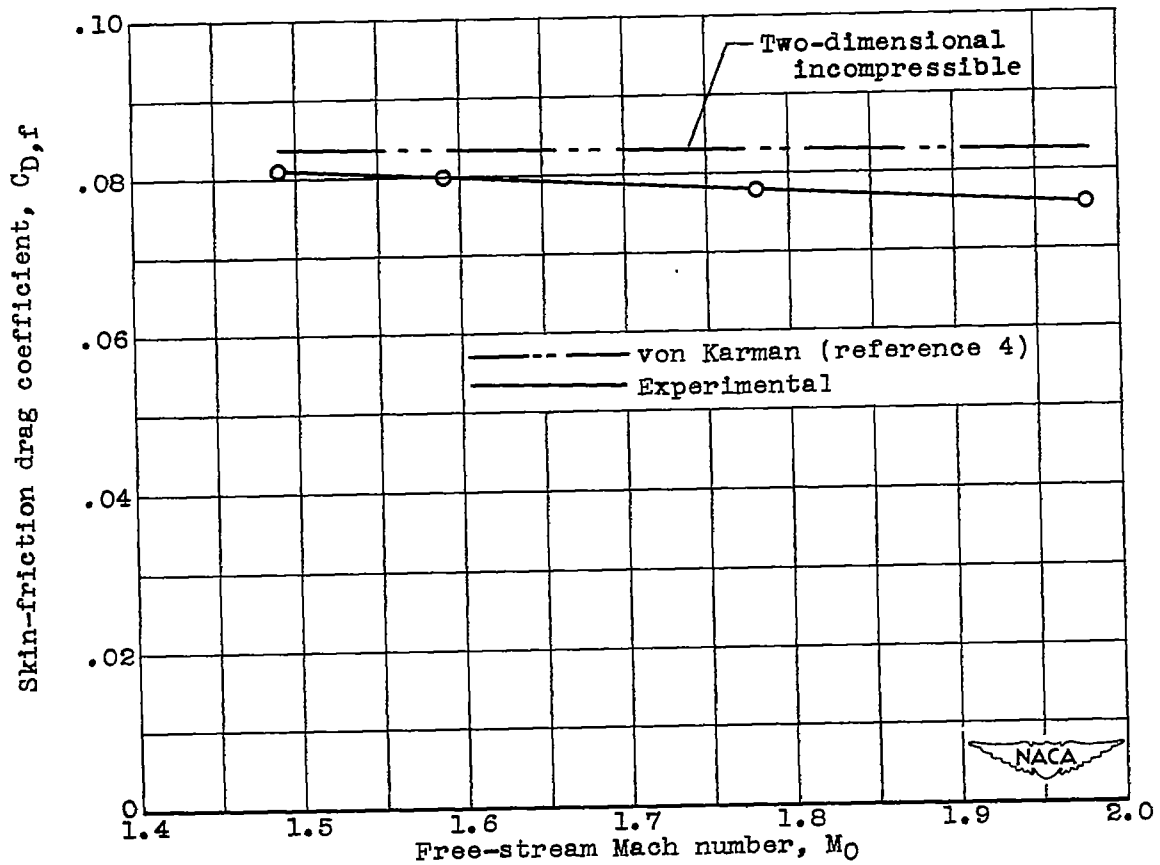


(d) Drag coefficient.

Figure 4. - Concluded. Variation of aerodynamic characteristics with Mach number at various angles of attack for body alone.



(a) Pressure drag coefficient.



(b) Skin-friction drag coefficient.

Figure 5. - Comparison of variation of theoretical and experimental drag coefficients with Mach number for body alone at zero angle of attack.

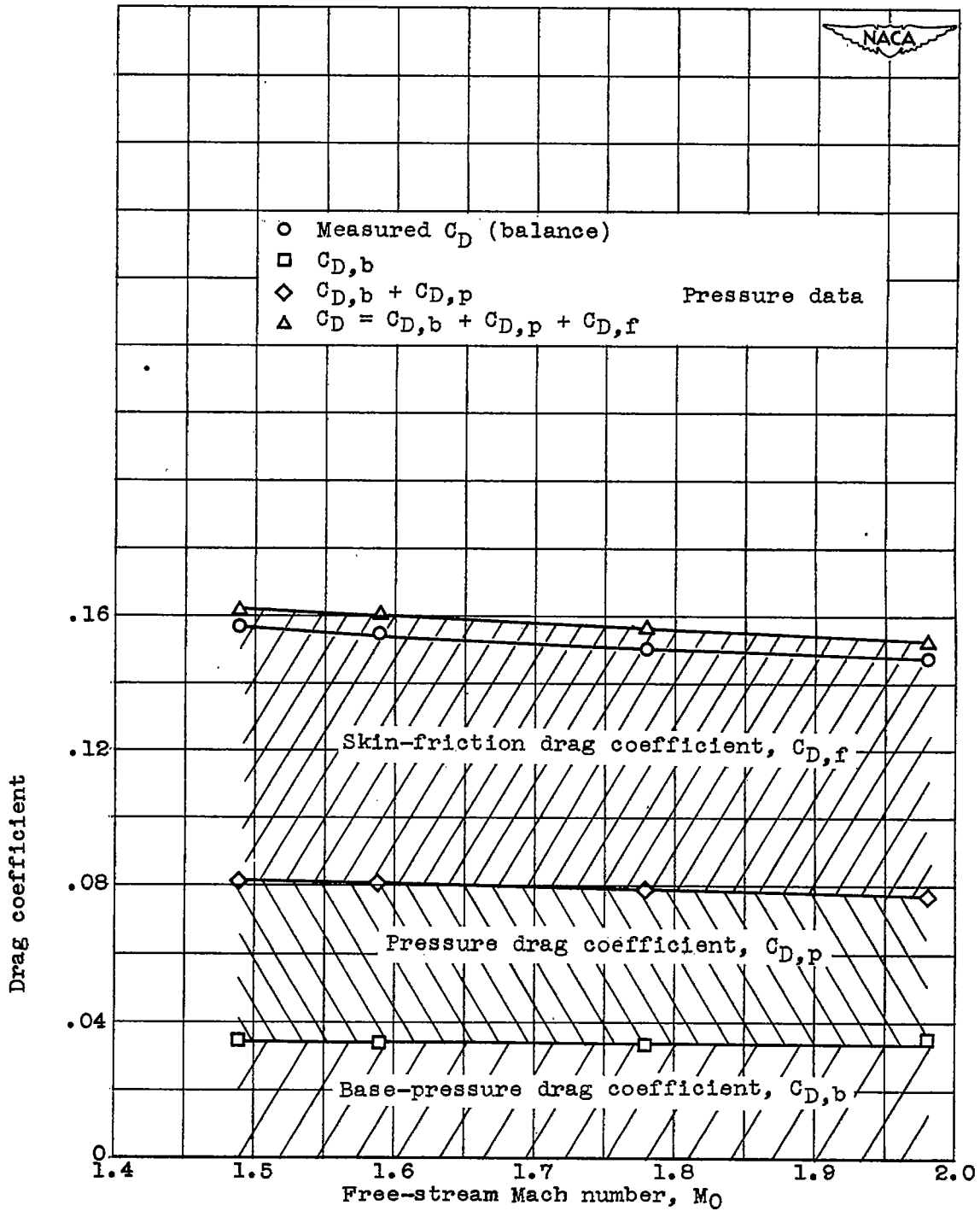
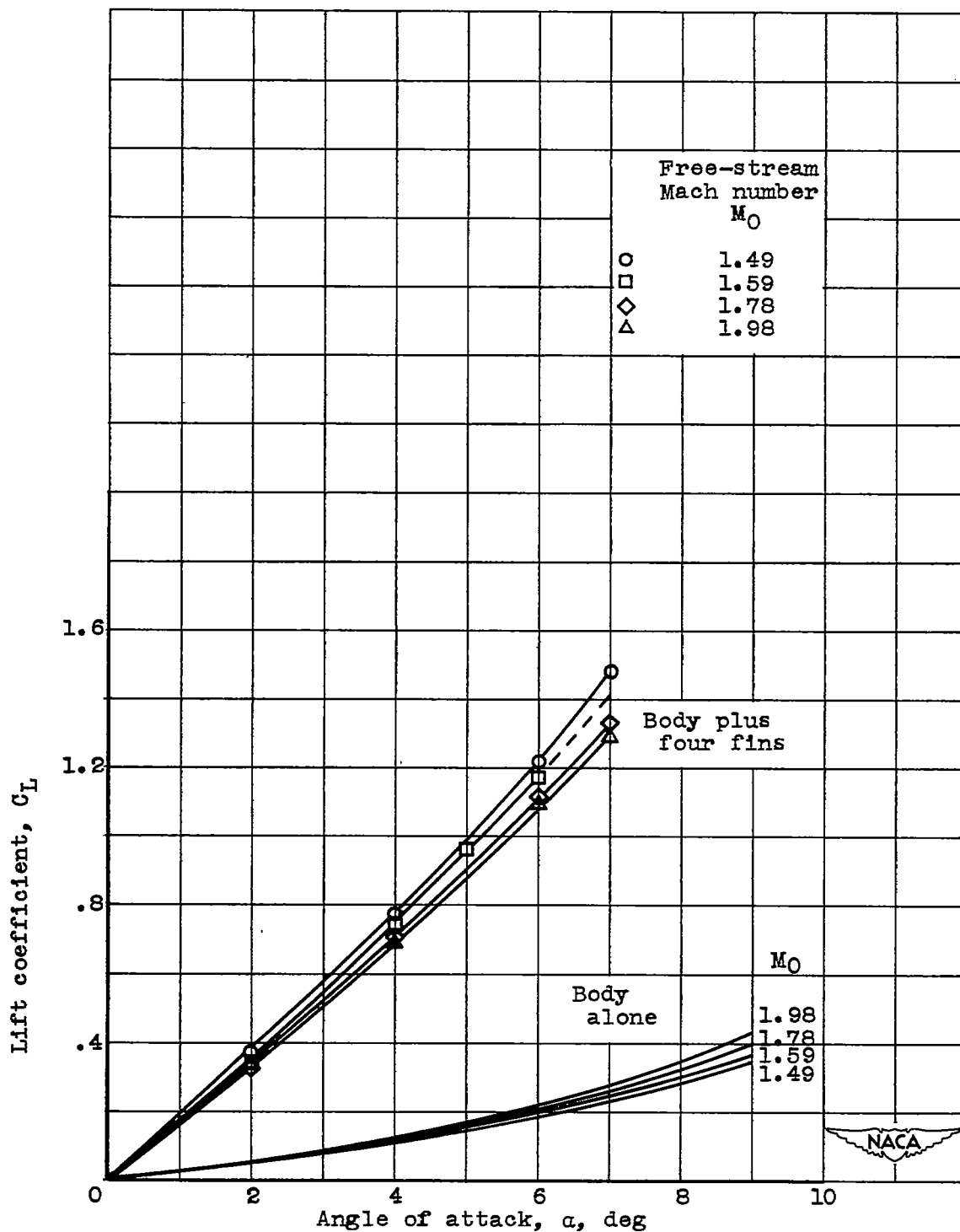
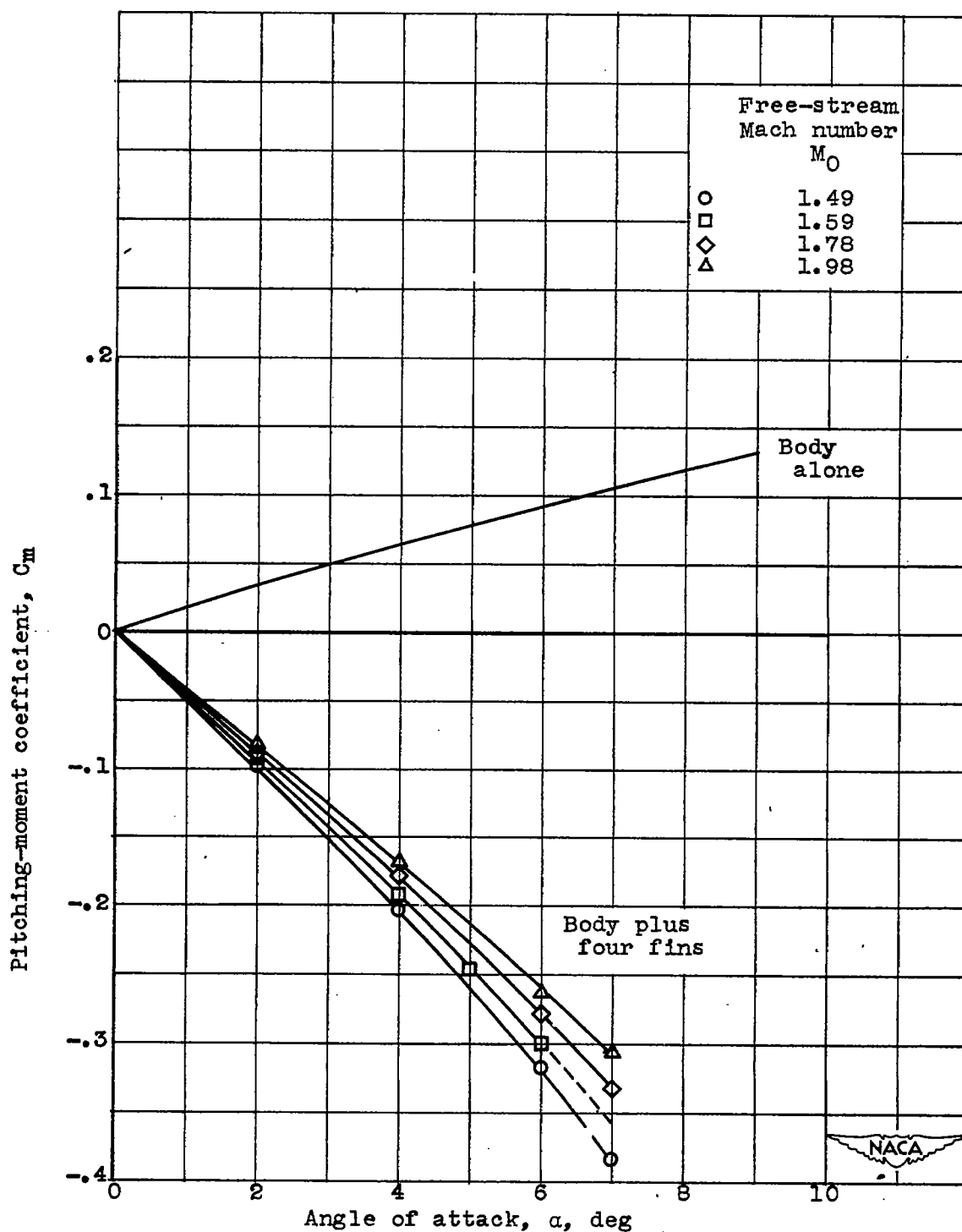


Figure 6. - Variation of components of drag coefficient with Mach number at zero angle of attack for body alone.



(a) Lift coefficient.

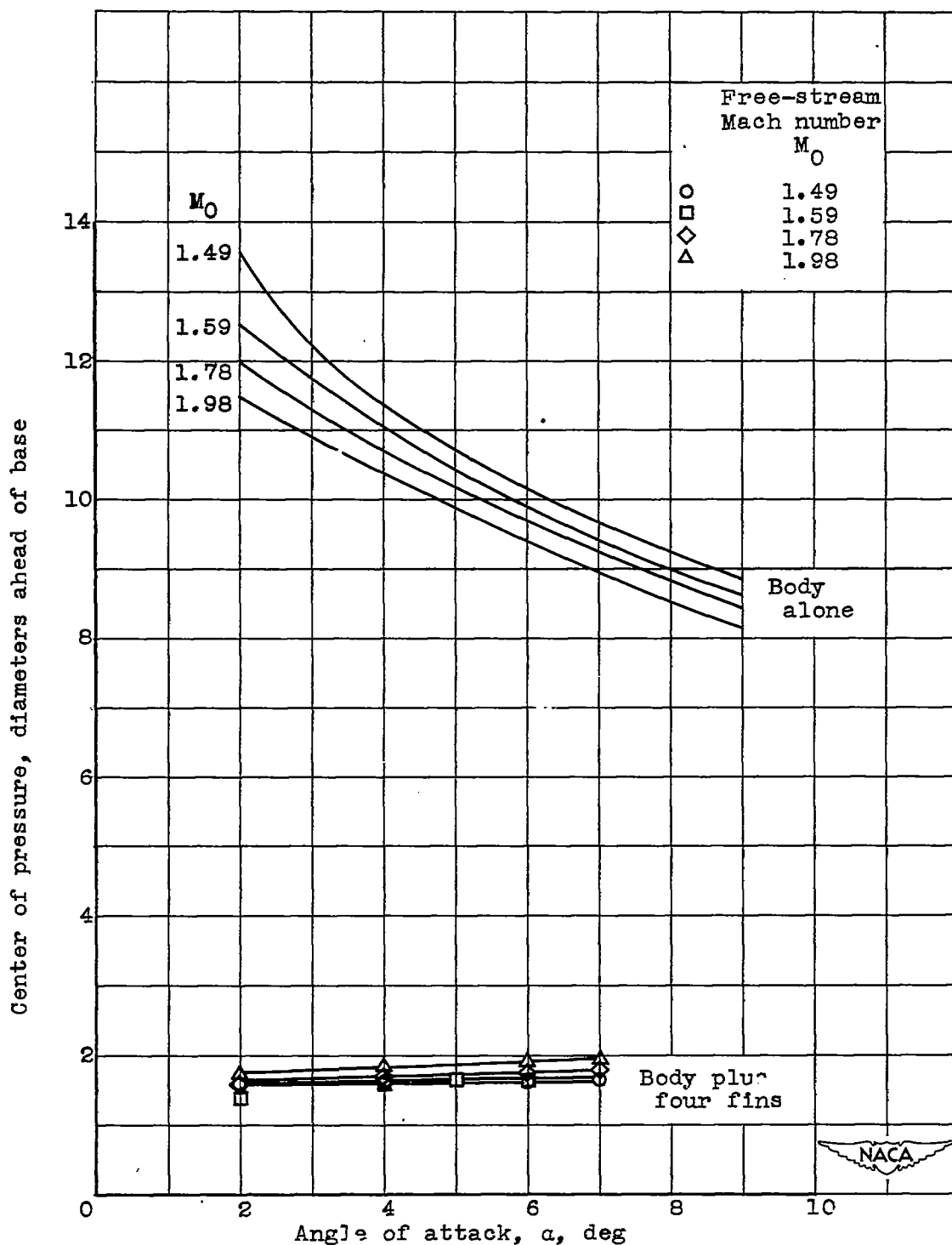
Figure 7. - Variation of aerodynamic characteristics with angle of attack at four Mach numbers for body plus four fins.



(b) Pitching-moment coefficient.

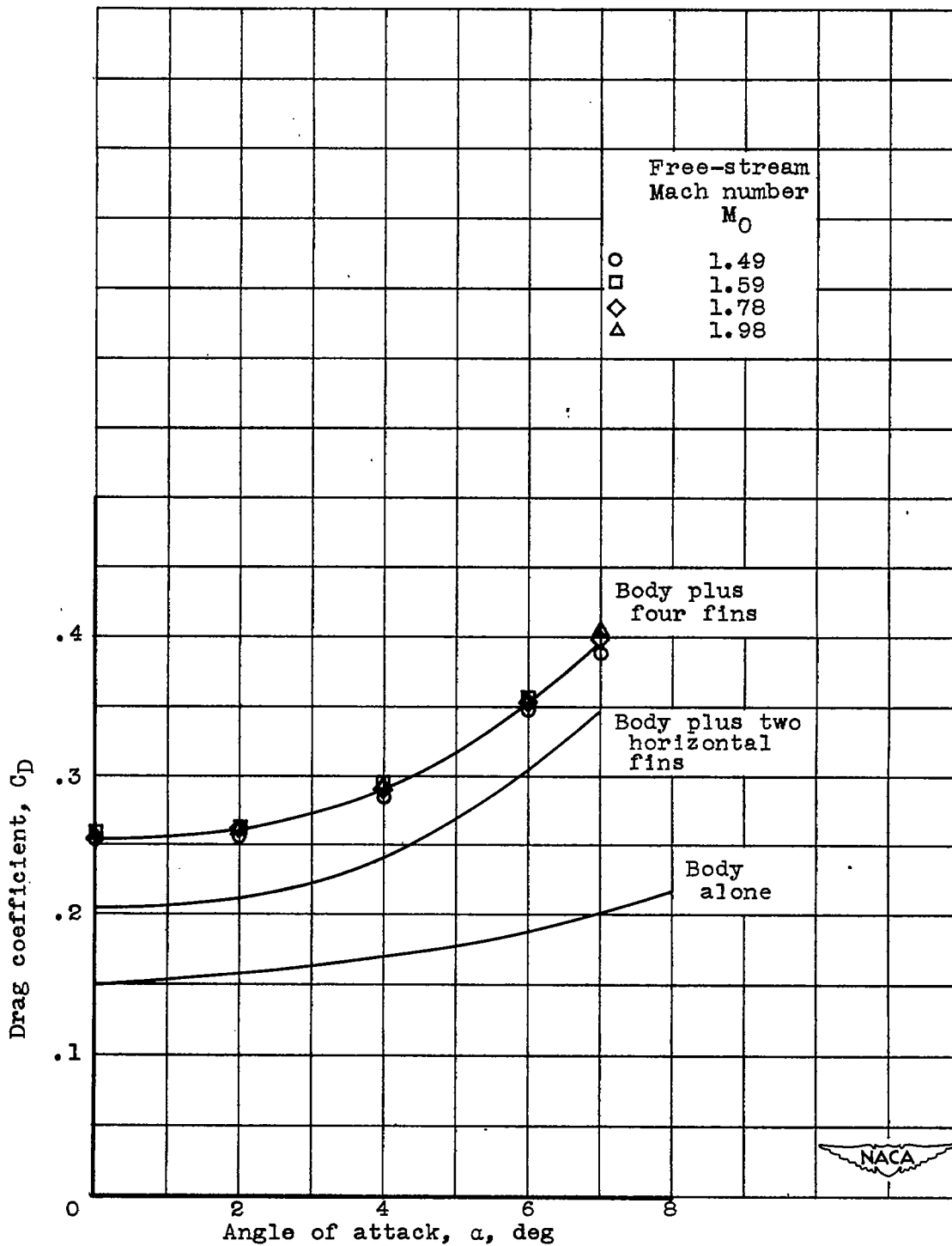
Figure 7. - Continued. Variation of aerodynamic characteristics with angle of attack at four Mach numbers for body plus four fins.

1315



(c) Center of pressure.

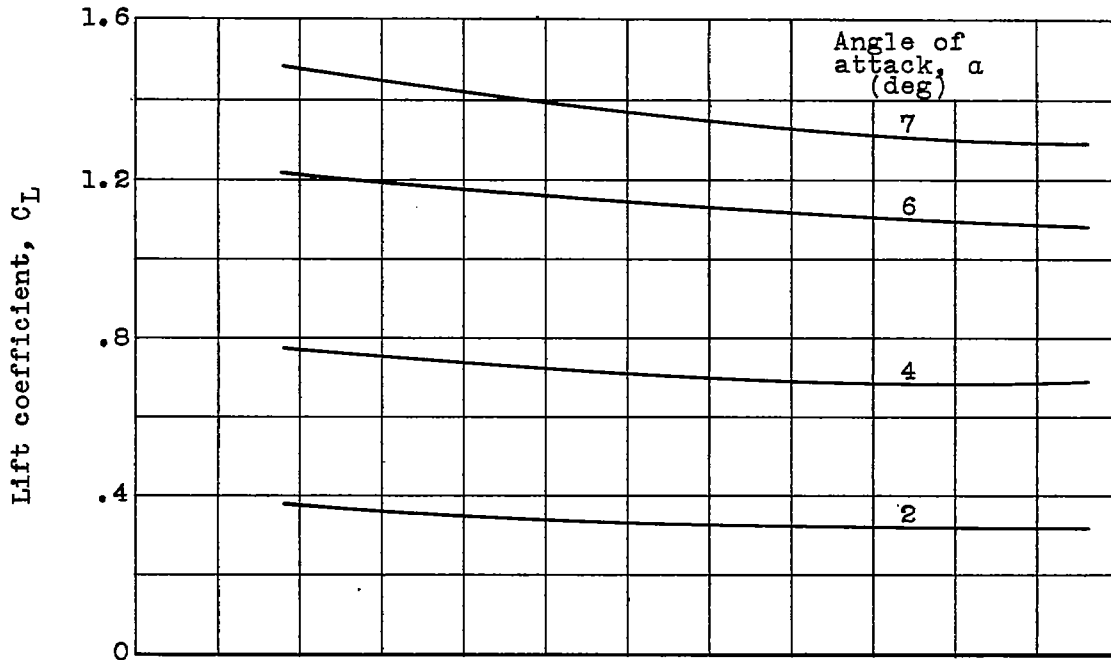
Figure 7. - Continued. Variation of aerodynamic characteristics with angle of attack at four Mach numbers for body plus four fins.



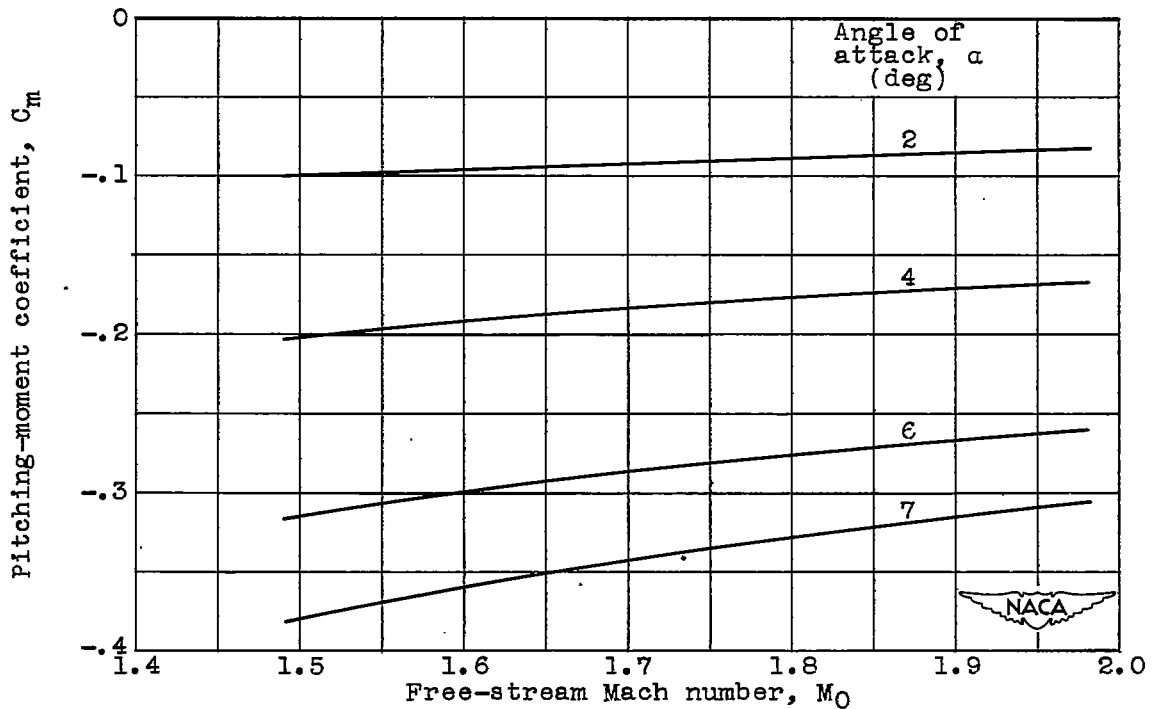
(d) Drag coefficient.

Figure 7. - Concluded. Variation of aerodynamic characteristics with angle of attack at four Mach numbers for body plus four fins.

1315

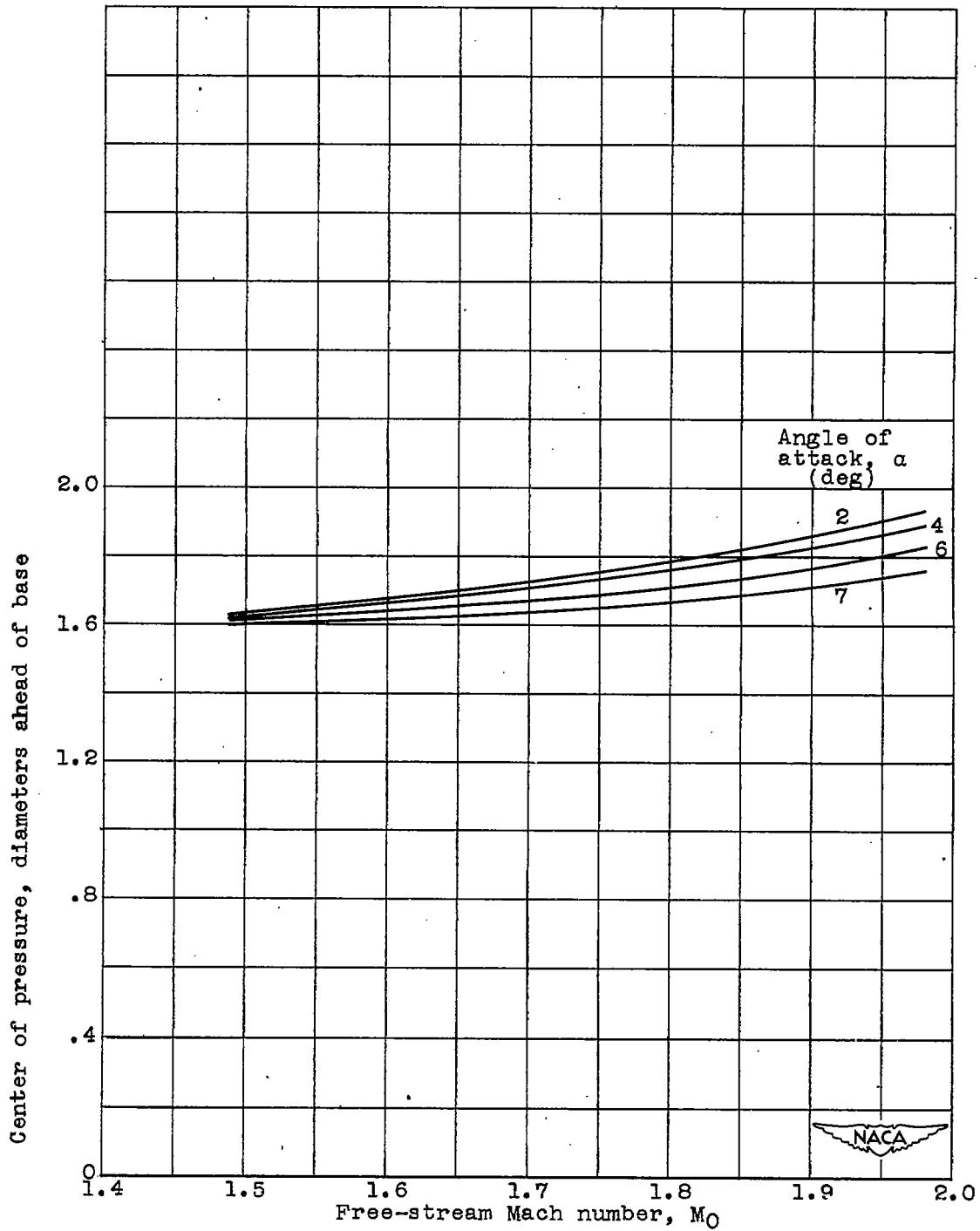


(a) Lift coefficient.



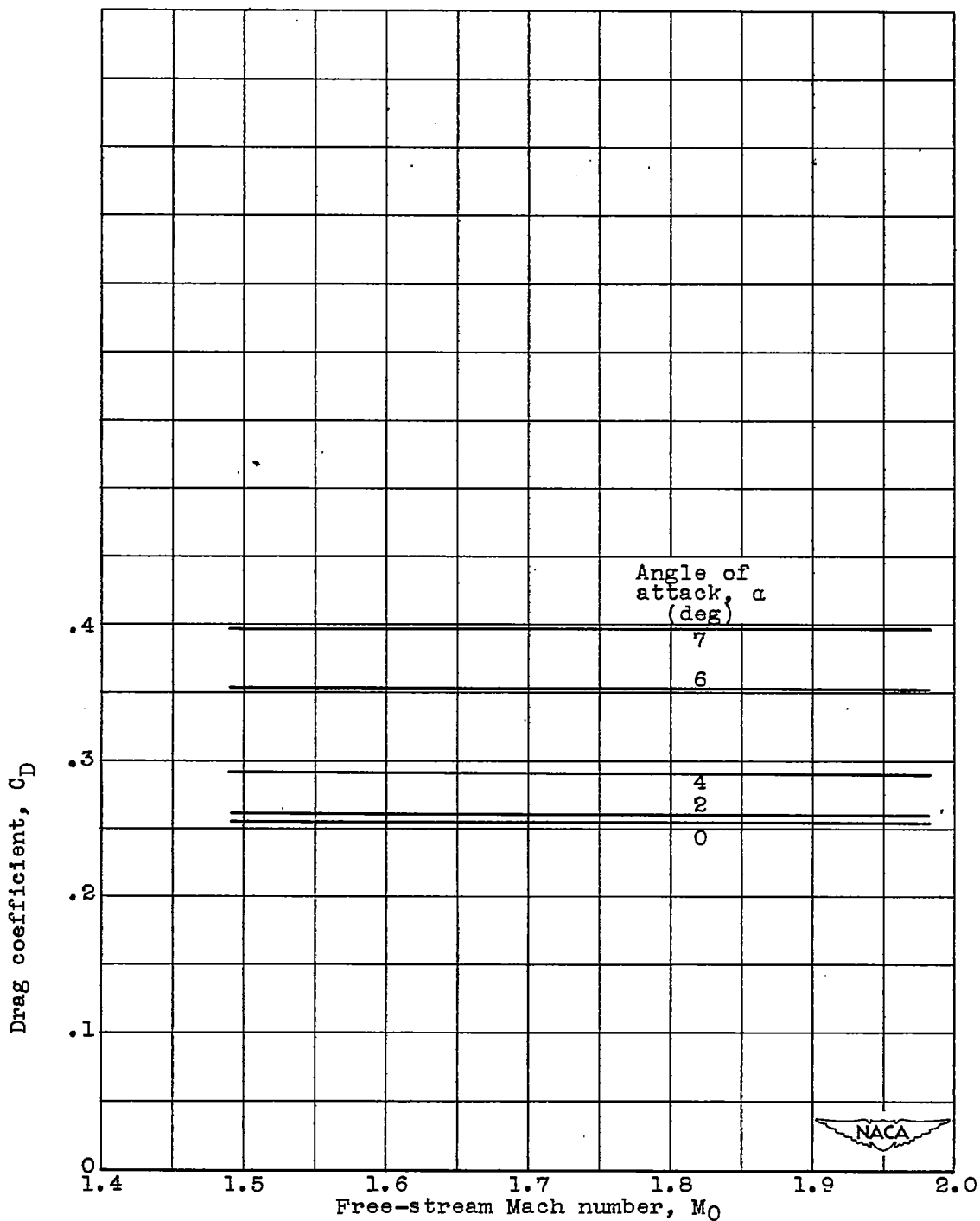
(b) Pitching-moment coefficient.

Figure 8. - Variation of aerodynamic characteristics with Mach number at various angles of attack for body plus four fins.



(c) Center of pressure.

Figure 8. - Continued. Variation of aerodynamic characteristics with Mach number at various angles of attack for body plus four fins.



(d) Drag coefficient.

Figure 8. - Concluded. Variation of aerodynamic characteristics with Mach number at various angles of attack for body plus four fins.

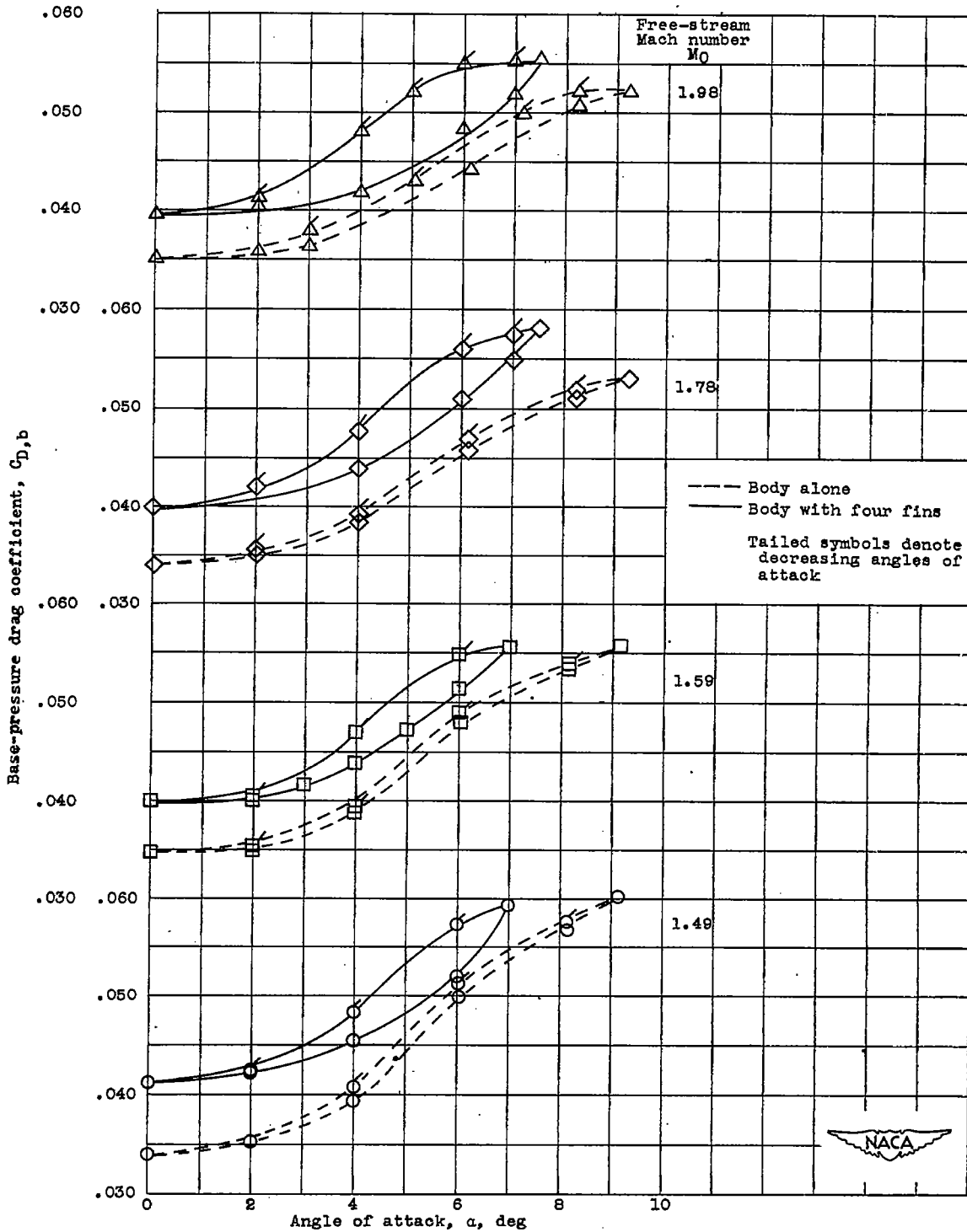


Figure 9. - Variation of base-pressure drag coefficient with angle of attack at four Mach numbers for body alone and body with four fins.